Aquacultural Engineering 87 (2019) 102018

Contents lists available at ScienceDirect

Aquacultural Engineering

journal homepage: www.elsevier.com/locate/aque

Review

Determining spatial feed distribution in sea cage aquaculture using an aerial camera platform

Andreas Myskja Lien[a,*], Christian Schellewald[a], Annette Stahl[b], Kevin Frank[a], Kristoffer Rist Skøien[b,c], Jan Inge Tjølsen[d]

[a] SINTEF Ocean, 7465 Trondheim, Norway
[b] NTNU Department of Engineering Cybernetics, 7491 Trondheim, Norway
[c] SINTEF, Centre for Research Based Innovation in Aquaculture Technology (CREATE), 7645 Trondheim, Norway
[d] AKVA Group ASA, 4340 Bryne, Norway

ARTICLE INFO

Keywords:
Sea cage aquaculture
Spatial feed distribution
Atlantic salmon
Aerial camera system

ABSTRACT

Within this paper we describe an unmanned aerial vehicle (UAV) based method to estimate the spatial feed pellet distribution in salmon fish-cages and exploit it within a case study to determine the radial pellet distribution for different rotor spreaders and blower configurations. Compared to previously used methods, capturing pellets thrown from a rotary feed spreader in rows of Styrofoam boxes, the UAV based method is simpler and faster to setup and allows to cover a larger portion of the sea cage surface area. We compare results obtained with the Styrofoam box method with results we obtained by an automatic analysis of aerial videos taken by the UAV during feeding experiments. The employed method helps to gain insight into the spatial feed pellet distribution in full-scale salmon fish-cages where the feeding pipe and actual fixation of the spreader may influence the dynamic behaviour of the feeding system. This can also be seen as a step towards a continuous measuring of the feed pellet distribution, particularly in view of possible future feeding systems that may allow to adapt the feed pellet distribution to the actual fish distribution.

1. Introduction

1.1. Motivation

In Norway, production and export of salmon are key contributions to the economy and within the aquaculture production feeding represents currently the single most important cost factor. Optimizing the feeding is therefore of high commercial interest and requires a deeper understanding of the feeding process itself.

Within this paper we describe an automated method for estimating the spatial feed pellet distribution that results from rotor spreaders that are commonly employed in salmon fish cages. The aim of this study is to evaluate the effectivity of an experimental setup for measuring the pellet-distribution with an unmanned aerial vehicle (UAV) based camera system at a full scale fish farm. Basic image analysis is used to estimate the count of pellet droppings on the water surface.

1.1.1. Optimizing feeding

Optimal feeding aims to reach a maximum growth of the fish. Therefore, optimal feeding is characterized by the fact that all hungry fish are fed and that simultaneously a maximum of the feed is consumed by the fish, thereby minimizing feed pellet loss. Failing to do so might result in one or several of the following issues; underfeeding, reduced growth, increased stress due to increased competition among fish, a larger size variation and nutrient discharge to the environment (Einen et al., 1995; Kadri et al., 1996; Noble et al., 2008; Talbot, 1993; Talbot et al., 1999) all leading to economic losses for the fish farmers. Reduced fish welfare is also directly linked to reduced feed intake and growth (Attia et al., 2012; López-Olmeda et al., 2012). Thus, when feeding large populations of fish in sea cages, it is anticipated that spreading the feed pellets uniformly and over a large area is beneficial (Attia et al., 2012; Juell, 1995; Kadri et al., 1996; Metcalfe and Thorpe, 1992; Olla et al., 1992; Thomassen and Lekang, 1993). The underlying thought is that the feed pellets should be delivered in a way such that the fish can find and eat the pellets, at a rate adapted to the appetite of the fish (Talbot et al., 1999). Currently the main uncertainty related to the feeding process is associated to the uniformity of the surface coverage of feed pellets distributed with currently used rotor spreaders.

* Corresponding author.
E-mail address: andreas.m.lien@sintef.no (A.M. Lien).

https://doi.org/10.1016/j.aquaeng.2019.102018
Received 7 December 2018; Received in revised form 21 August 2019; Accepted 18 September 2019
Available online 17 October 2019

1.1.2. Commercial background

Farmed production of Atlantic salmon (Salmo salar) has increased from 297 to over 2.3 million tonnes globally from 1970 to 2014 (FAO, 2015) and continues to follow this trend. In 2016, the Norwegian aquaculture industry produced Atlantic salmon and rainbow trout at 978 sea based sites with a total product value of 6.7 billion EUR (Sandberg and Steinseide, 2017). The cost of feed represents about 50% of all expenses (Winther et al., 2011) and 1.6 million tonnes of feed were administered at Norwegian salmon and trout farms in 2016.

At a feed price of about 1.2 EUR/kg in 2016 (Norwegian Directorate of Fisheries, 2013) this corresponds to a total value of about 2 billion EUR. While in the sea, the cage fish is fed a diet mainly consisting of a mixture of soy protein concentrate, rapeseed oil, fish meal, fish oil and wheat starch (Ytrestøyl et al., 2014) in the form of a 3-12 mm diameter pellet adapted to the current size of the fish.

1.2. Related work

Some models have been developed previously to describe the pellet distribution from a rotor spreader on the surface and in the water along with the simulation of fish behaviour and feeding in salmon cages (Alver et al., 2004, 2016; Føre et al., 2009). In order to provide input to such models, experiments have been conducted to investigate the spreading by counting pellets landing in two rows of Styrofoam boxes on the water surface. The results showed that the distribution was annular (ring-shaped), often skewed to one side, and covered a limited percentage of the sea cage surface area (Oehme et al., 2012). The Styrofoam box method is simple, but it conceptually covers only a small portion of the surface area, requires weighting or photographing and counting. In addition the boxes are difficult to put and hold into position within a real sea cage. Therefore, there is a need for alternative methods which are simpler, faster and which can be applied to a wide selection of spreader designs including future spreaders that may allow for a more targeted spreading of the pellets.

The solution we investigate in this paper exploits the automated analysis of videos recorded by an UAV. An experiment also using an UAV was performed by Skøien et al. (2016a), however their manual counting analysis was restricted to a small cross section emulating the area previously covered by Styrofoam boxes. Note that compared to the Styrofoam box method, which only cover limited segments, the method presented from this study can cover the entire water surface. However, the challenges lie in identifying pellets over a large area with varying lighting conditions from a single camera footage. In order to cope with different lighting conditions one often needs to employ thresholding techniques without introducing a user based bias. Many of these techniques are surveyed within (Sezgin and Sankur, 2004). Morphological filters (Soille, 2003) represent another important class of filters for Image Analysis and are often exploited for the extraction of "countable" objects in images. A broader overview into low-level computer vision (including feature detection and segmentation) which is useful for counting in images can be found in Szeliski (2010). To verify the method, the results are compared with a reference measurement obtained using the previous Styrofoam box method.

2. Materials and methods

2.1. Experimental setup

The experiment was conducted in the time period from the 4th to the 6th of August 2015 at the fish farming location *Korsneset* in the Halsa municipal in central Norway.

2.1.1. Cage and site-location

The fish farm has geographic coordinates 63°8′46,7″N, 8°13′17.5″E and a detailed map of this site is illustrated in Fig. 1. It is administered from a barge which is moored between cage nine and seven (Fig. 1). A circular High Density Polyethylene (HDPE) cage at the position labeled with number six (cf. Fig. 1) was used throughout the experiment. The circumference of the cage was 157 m, which is a typical size of Norwegian sea cages (Oppedal et al., 2011). No fish net was mounted to the cage and no fish was present during the duration of the experiment. A circular bird net frame (known as hamster wheel) with a circumference of 72 m was placed in the center of the cage (Fig. 2).

2.1.2. Feed distribution system

The feed barge contains an array of silos holding feed pellets which may be of different size and ingredient compositions. The particular pellet type used for all the experiments was a 9mm Optiline S L 2500-50A (Skretting, Stavanger, Norway). The pellet transport from the barge to the sea cage is performed pneumatically using blowers (Omega CB131 C, Kaeser Compressors, Inc., Fredericksburg, VA, USA) which are able to move 10.85 m^3/min of air at up to 1 bar pressure difference. The feed pellets are transported through a high-density polyethylene (HDPE) pipe with an outer diameter of 90 mm and a wall thickness of 7 mm. The pipe length measured 317 m from the selector valve on the barge to the rotor spreader. The feed pipe was tied to the floating collar in such a way that the pipe was as straight as possible from the edge of the hamster wheel towards the centre of the cage, where the rotor spreader was moored. The feed pipe terminates in a rotor spreader (cf. next Section 2.1.3), centrally placed, which spreads the pellets across the water surface. Both the pellet throw and the rotation of the spreader are driven by the same airflow, and the latter arises due to the spiral shape of the outlet pipe. This design is popular among fish farms and is often used due to its simplicity, low cost and low maintenance. Variants of this spreader type can be found across the world.

2.1.3. Rotor spreaders used in the experiment

The particular rotor spreaders we used within our case study were the AKVA Group "CF90 Double" and the AKVA Group "Hex Base". Both spreaders are commonly used in sea based salmon aquaculture (Skøien et al., 2015) and consist of a 90° bent steel pipe, where the lower end is connected to the feed pipe, and the upper part is connected to a bearing. The bearing allows the upper lightweight aluminium pipe (center pipe) to rotate, spreading the feed pellets in an annular pattern (Oehme et al., 2012). At the end of the center pipe there is also an adjustable spout allowing for an alteration of the pellet trajectory. Both spreaders were tested with an aluminium center pipe with a bend radius of 600 mm, in our experiments referred to as **C600** for the "CF90 Double" and **H600** for the "Hex Base". The "Hex Base" spreader was additionally tested with a center pipe with a bend radius of 450 mm, to which we refer to as **H450**. The three used spreader instances are shown in Fig. 3.

All used spreader pipe outlets have an upwards angle of 15° with respect to the horizon. The spreader design differs in that the "CF90 Double" is kept floating by a buoy attached directly below the bearing on a shaft, and a counterweight at the bottom end of the shaft is maintaining the spreader in an upright position thereby counteracting the roll and pitch of the spreader, whereas the bearing of the "Hex Base" spreader is supported by three equally spaced HDPE support beams attached to a hexagonal floating frame that consists also of HDPE pipes arranged in a hexagonal shape thereby maintaining the stability of this spreader type.

2.2. Data acquisition

In order to record the pellets that drop with a splash into the water, we used a UAV to record aerial videos from a top-view position of the hamster wheel in the fish cage. For comparison, we performed a manual reference measurement during one of the experiments by placing and arranging Styrofoam boxes in a cross-formation onto the water surface. Both the UAV recordings and manual Styrofoam box sampling are described below in more detail.

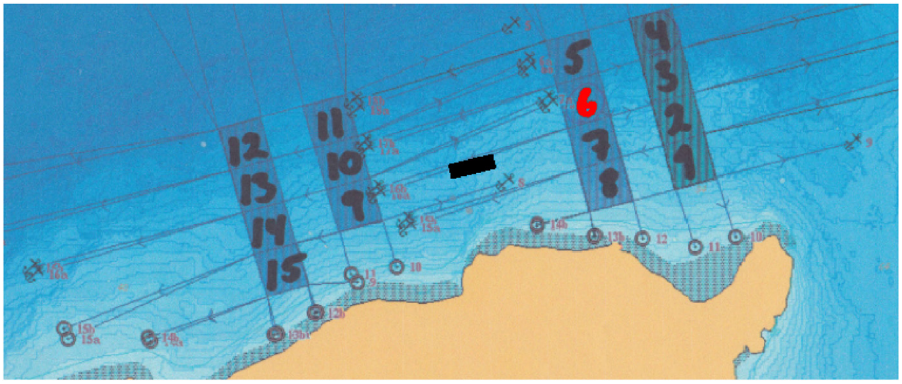

Fig. 1. Overview of the site. The fish farming site Korsneset with cage number indications. The experiment was conducted at cage 6. The position of the feed barge is indicated between cage 9 and 7.

Fig. 2. The experiment cage, i.e. the floating collar along with the *centered* circular bird net frame (hamster wheel) is shown in the foreground. Also the feed barge can be seen in the background (top-left corner), as well as the white feed pipe running between the barge and the cage.

2.2.1. Aerial image capture details

The image sequences were captured using an Unmanned Aerial Vehicle (UAV), Dji Inspire 1 UAV (Shenzhen, China). The UAV was positioned directly above the rotor spreader at a height of 25.85 m. The UAV carried a 4 K camera with 94° FOV, a lens with 9 elements in 9 groups, and a 1/2.3 inch CMOS sensor in a 3-axis stabilization gimbal. The images were shot at 25 FPS with an image resolution of 4096 × 2160 pixels. The camera was calibrated using a 7 × 9 (A4) checker-board calibration pattern. The gimbal was set to point the camera straight down, perpendicular to the water surface. It is assumed that this camera orientation was maintained throughout the experiment, hence avoiding the need to compensate for the roll and pitch of the UAV.

2.2.2. Styrofoam box sampling

For comparison, during the C600 spreader experiment, we also sampled the pellet distribution using Styrofoam boxes (Bewi AirBOX). The size of a single Styrofoam box was 0.4 m × 0.8 m and the boxes were mounted in four radial arrays with a separation angle of approximately 90°. Each row consisted of 26 boxes connected on the long edge by plastic clamps. The first row was aligned along the feed pipe. Fig. 4 shows a top-view of the hamster wheel containing the rows of the Styrofoam boxes. Note that no pellets were observed to land outside of the hamster wheel and the Styrofoam boxes were therefore placed only in the inner part of the hamster wheel covering the radius from the rotor spreader to the inner edge of the frame. Each box was marked with a unique ID number in the bottom for a later identification within

Fig. 3. Rotor spreaders used in the experiment. From left to right: CF90 Double with 600 mm bend radius center pipe (C600), Hex Base with 600 mm bend radius center pipe (H600), Hex Base with 450 mm bend radius center pipe (H450) (illustrations by courtesy of AKVA Group AS).

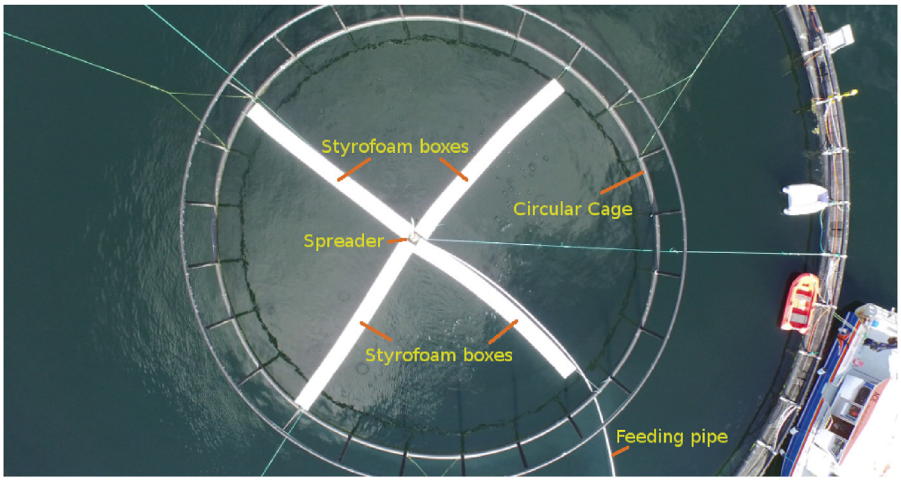

Fig. 4. Overhead footage taken from the UAV. The rotary spreader is located in the centre of the image with the feed pipe entering from the top. Four rows of Styrofoam boxes are visible, with the two vertical rows running along the direction of the feed pipe, and the two horizontal rows running perpendicular to the direction of the feed pipe.

the images.

2.3. Experiments

The actual experiments were performed in batches for the three rotor spreader configurations i.e. C600, H600 and H450 (cf. Section 2.1.3). Note that the Styrofoam boxes were only used during experiments with the C600 rotor spreader. Before running the H600 and H450 experiments, the boxes were removed. A single spreader experiment started with a pure airflow of about 20 s before the feed pellets were released from the silo into the feed pipe. This ensured that the spreader rotation speed was already stable enough to prevent data skew caused by slow airspeed at the beginning of tests. The UAV captured aerial images during the entire feed batch delivery, and docked on the research support vessel in-between experiments. After each batch for the C600 experiments the content of every Styrofoam box was photographed for later counting of pellets and emptied before the start of the next batch. Two different airflow speeds were used in the experiments; 16 m s^{-1} and 20 m s^{-1}. Three replicate experiments were run for each air speed. Each consisted of one batch of feed pellets delivered at 20 kg/min for 1 min. Wind speed and direction was also recorded during each test using a 7N1 V10 anemometer (TFA, Dostmann GmbH & Co. KG, Wertheim, Germany).

The mean pellet speed through the feed pipe was measured by taking the time from the first pellets entering the feed pipe, to their exit at the rotor spreader.

2.4. Data analysis

2.4.1. Reference coordinate system and virtual box segments

For the evaluation and comparison of the experiments we introduced a reference coordinate system that has its origin in the center of the spreader, the positive x-axis goes along the feed pipe – away from the spreader – and the z-axis is pointing down towards the sea (compare (Skøien et al., 2015, 2016b)). For image processing analysis and pellet density illustration, the water surface was divided into 800 virtual sectors: 25 divisions in the radial direction and 32 in the circumferential direction (Fig. 5). For comparison with the Styrofoam box measurements, we also defined two perpendicular virtual box arrays with 26 box segments of rectangular shape that emulated the Styrofoam boxes with a size of 0.4 m × 0.8 m.

2.4.2. Styrofoam box pellet count

We counted the pellets in the Styrofoam boxes semi-automatically from the photos taken during the experiment using the open source image analysis software OpenCFU (Geissmann, 2013). A 4-point convex polygon region of interest – enclosing the visible bottom of the box – had to be defined to avoid pellet counting from adjacent boxes. No image pre-processing like noise-filtering was necessary and standard local thresholding (with a radius of 15 to 20 pixels) led already to a robust identification and counting of separated individual pellets. However, a manual count correction was necessary for pellet clusters that appeared when several pellets gathered tighter together (see. Fig. 6).

2.4.3. Image processing

The aim of the image sequence analysis of the aerial videos from the UAV-camera is to determine the spatial pellet distribution based on the visible splashes that appear when the pellets hit the water-surface. An assumption we make is that the splash-activity is proportional to the number of pellets that hit the surface. Single pellets create usually a countable splash that is visible for a few frames, however pellet-clusters result in larger not-countable areas of splash-activity and the splash surface area is taken as indicator for the amount of involved pellets. The different weather conditions lead to largely varying reflections on the water surface and the main image processing based challenges arise due to these different and often quickly changing lighting conditions. Fig. 7 shows the top-view images from the 3 different experiments. The first left image shows an image during a C600 experiment and due to a gray cloudy day the water surface appears uniformly gray. Compared to the weather conditions during the other two experiments (brighter days with some clouds) this represented the best and therefore preferred condition for an automatic detection of the pellet splashes.

In Fig. 8 a typical top-view image from a video taken by the UAV-camera during the C600-experiment is shown. Here the rotating spreader is located in the centre of the white “cross” that consists of concatenated Styrofoam boxes and lies within the circular frame of the hamster wheel. The feeding pipe comes in from the lower right side of the cage. Our aim was to analyze the video data such that we can measure the position and size of the splashes from the dropping feed pellets relatively to the rotating spreader. For this the position of the rotating spreader and the feeding pipe orientation was marked manually within the videos and used to set the origin and the x-axis of the reference coordinate system. The absolute scale in the image at water level was determined by the known distance between two poles of the hamster wheel. A virtual circular surface disk of about 10 m was divided into the angle-radius-segments in which we measure the accumulated splash activity (compare Fig. 5).

2.4.4. Splash activity detection

When the pellets hit the water-surface usually a bright splash is visible for about 4–7 frames and in our approach we detect and count the splash pixels that are brighter than the near neighborhood. As the images/videos are taken outdoors in a natural environment we also had

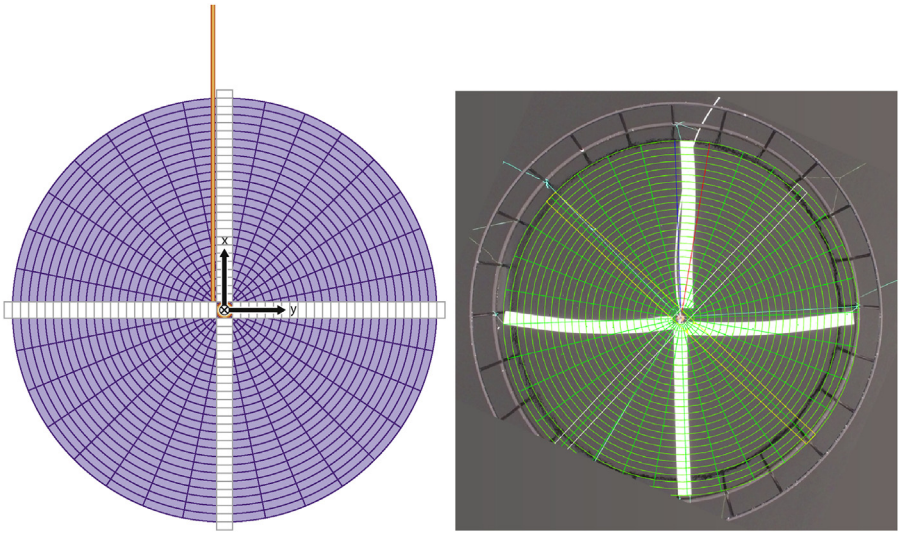

Fig. 5. The origin of the coordinate system introduced for reference was placed at the center of the spreader, positive *x*-axis along the feed pipe (orange) away from the spreader, and *z*-axis pointing towards the sea. The water surface was divided into 800 sectors (violet), 25 in the radial direction – corresponding to the width of the Styrofoam boxes (white) – and 32 in the circumferential direction. (For interpretation of the references to color in this figure legend, the reader is referred to the web version of this article.)

to deal with the quickly changing lighting conditions – mainly induced by the reflection of clouds on the water-surface and possibly due to slight changes in the camera position – in an adaptive way. In a pre-processing step we compute the running mean (with an update rate of 0.05 for a new video frame) in order to capture the brightness-changes on the water surface adaptively. The difference image between this running mean and the current image frame captures then short time image changes like the occurrence of splashes quite well and helped to compensate for the illumination changes due to cloud-reflections and/or water-brightness-changes. Then the splashes of the dropping pellets have to be identified and extracted in order to count or measure the splashes/splash-areas relative to the spreader in the images. For this a morphological "top-head" image processing step followed by a thresholding is employed on the difference image to extract the brighter pixels that correspond to the splashes. A masking of the rigid hamster wheel along with the more flexible ropes helps to avoid to identify small motions or changes at the border of these structures wrongly as splashes. Using the initial spreader position as centre-point and the predefined radius to the hamster wheel we divide the circular neighborhood into angle-radius segments within which we count the pixels that are classified as a splash in the water. Normalizing this, we can compute and illustrate the measured probability density for the splash activity (Fig. 9).

3. Results

Analyzing the splash activity from the UAV videos we could determine the spatial pellet distribution of the used spreaders. An example for the C600 experiment at an air speed of 20 m s^{-1} is illustrated in Fig. 10. Note that the pellet splashes detected were normalized and for each of the sectors were adjusted by an areal factor (divided by the area of the respective sector), so that the color coded display reflects the density of the pellet distribution. A main characteristic of the observed pellet density is the non-uniform distribution of pellet splashes during the observed time-period. This mainly comes from the fact that the pellets often come out of the spreader pipe in clustered batches with a

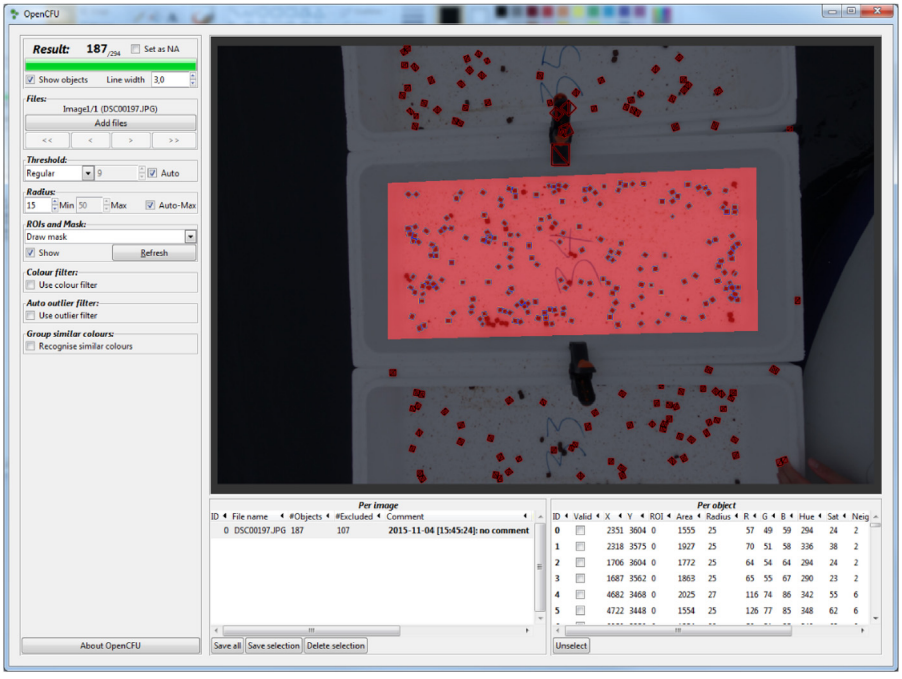

Fig. 6. OpenCFU was used to semi-automatically count the pellets in the images of the Styrofoam boxes. Pellet clusters required a manual correction of the count.

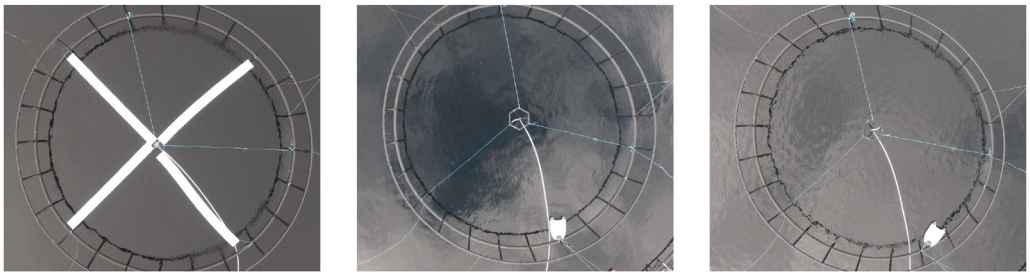

Fig. 7. Topview images of the hamster wheel of the fish cage taken by the UAV-camera for the C600, H600 and H450 pellet rotor spreader experiments. For an automatic video analysis the changing weather conditions led to challenging lighting conditions. For an automatic detection of the splashes the gray cloudy day resulted in a uniformly gray water surface and worked best for an automatic detection of the splashes.

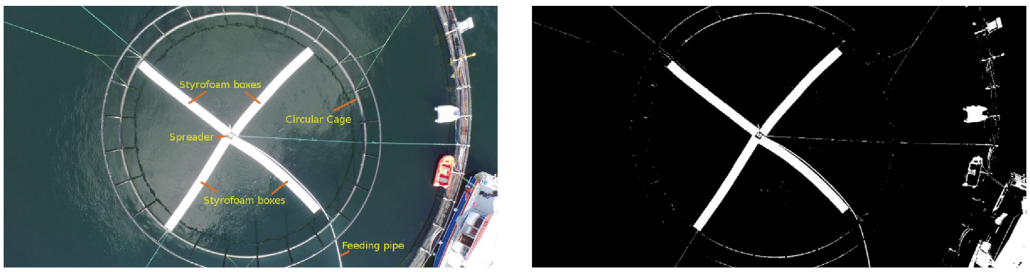

Fig. 8. Left: Topview image taken during a C600 spreader experiment by the UAV-camera. The main visible structures are labeled. **Right**: A threshold applied to the intensity values of the image is used in further post-processing to exclude structures that may falsely be seen as splashes.

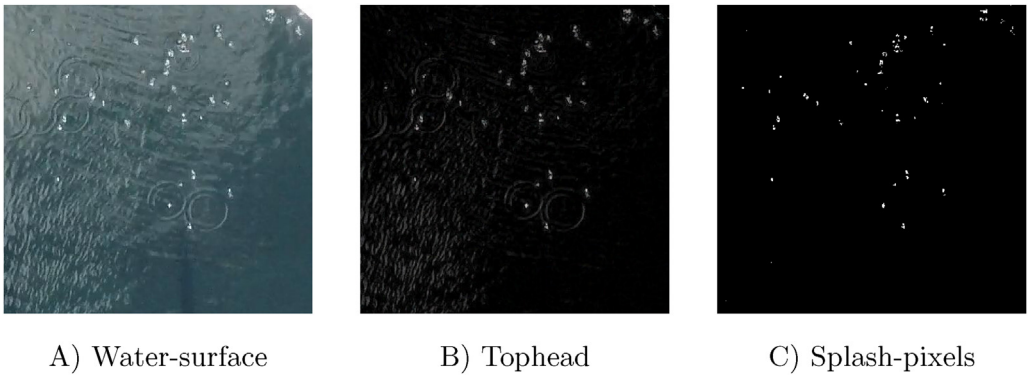

Fig. 9. (A) Top view of the water-surface with some pellet splashes and varying lighting conditions. (B) The resulting splash activity image after illumination correction and the application of a morphological top-head filter. (C) Pixels counted as showing splash activity.

high pellet density. The distribution for the other experiments show a very similar characteristic and we basically analyze the data based on the mean radial distribution. That means we compute the mean distribution in radial direction by gathering the pellet splashes over the whole 360° circle. Note that the observed rotor spreader rotation speed was largely dependent on blower air speed. An increase in blower air speed of 25% from 16 m s^{-1} to 20 m s^{-1} increased the rotation speed of the 600 mm bend radius pipes with approximately 26% and the rotation speed of the 450 mm bend radius pipe with approximately 43%. The H600 had a slightly higher rotation speed than the C600. This is likely due to the C600 being less stable in the water making the movement hindering a smooth rotation. The H450 had much higher rotation speed than the other models due to the total mass being lower and the center of mass being closer to the rotation axis (Table 1).

Below, we first compare the results we got by the Styrofoam box method with the image analysis results and then summarize the data obtained for all spreader configurations.

3.1. Comparing aerial images and the Styrofoam box method

In order to compare the two methods, namely the aerial image analysis and the Styrofoam box pellet count method, the first experiment with recordings of the C600 spreader were performed using both methods simultaneously. Note that in that case pellets landing in the Styrofoam boxes could not be detected by the image analysis, because they were not landing in the water, ergo no splash appears. But more relevant is that the white boxes appear very bright in the images, making any pellet detection in these overexposed image-areas impossible. The lack of splash detections within sectors covering or overlapping the box rows is reflected in the fact that no or lesser pellet density is measured in these areas. In Fig. 10 this can be seen in the color plots as sectors with colder color (blue) running radially from the center and outwards. An estimate for each of the sectors where the boxes were present were therefore made using the average splash detection numbers between the adjacent sectors on either side circumferentially. The comparison was performed using normalized numbers (Fig. 11). The characteristic of both distributions is reasonable similar thereby verifying that the aerial image analysis is equally suitable for determining the pellet spread. However we note that during the C600 experiment the lighting conditions for identifying the surface splashes were better than for the other two experiments.

3.2. Pellet distribution

In order to analyze the pellet distribution across the water surface from the rotor spreader, all sectors in circumferential direction were combined resulting in a more robust radial distribution that is smoothing the non-homogeneous spreading effects. This in turn allows

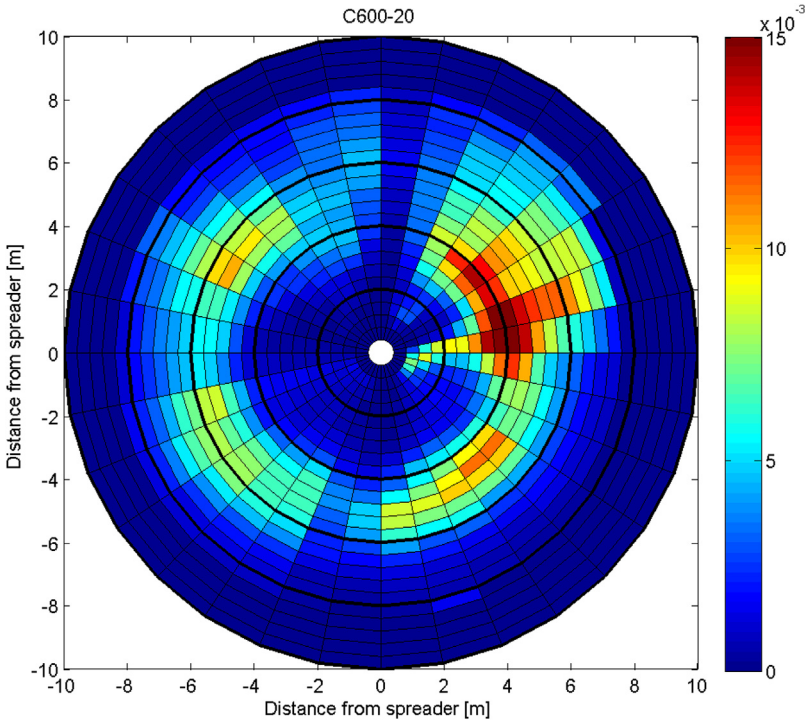

Fig. 10. Pellet splash detections on the water surface for the C600 experiment at an air speed of 20 m s^{-1}. Splash detections are normalized and divided by the area of the respective sector. Red colors represent a higher density of pellet splash detections. (For interpretation of the references to color in this figure legend, the reader is referred to the web version of this article.)

Table 1
Rotation speed of the spreader pipe in rounds per minute for the three rotor spreader models at blower air speeds 16 m s^{-1} and 20 m s^{-1}.

	16 [rpm]	20 [rpm]
C600	30	38
H450	46	66
H600	34	43

to quantify some key-variables that describe the distribution. We considered for each spreader configuration the area where 90% of the pellet splashes were detected. In particular the area was set between an inner limit, cutting off the 5% of splashes detected closest to the spreader, and an outer limit, cutting off the 5% of splashes detected furthest away from the spreader. That means that the distribution can be characterized by the inner limit radius and the outer limit radius which difference provides an approximate spread-range for the considered spreaders. In addition the center of gravity for the radial splash distribution was calculated as follows:

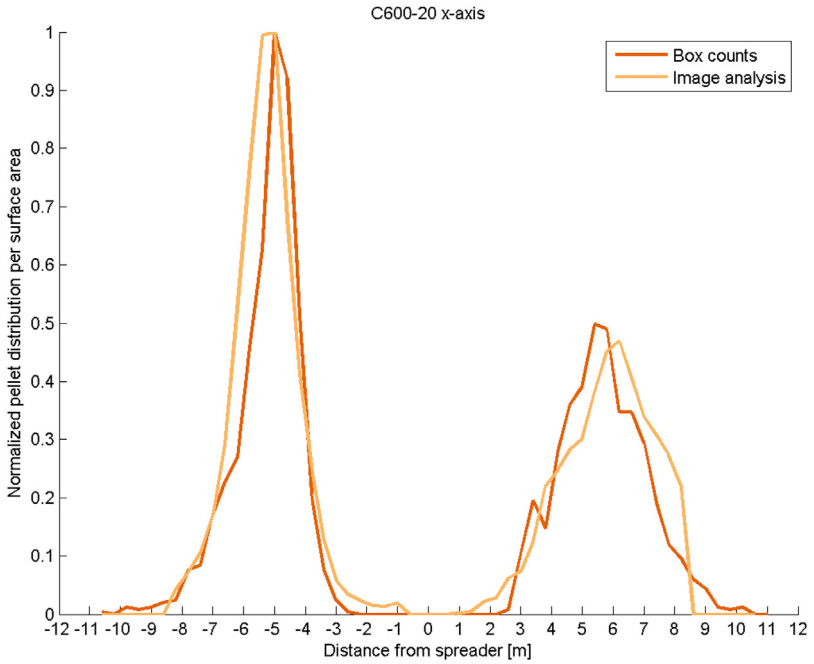

Fig. 11. Comparison between pellet counts in the Styrofoam boxes and an estimate of pellets landing in the same area using splash detections from aerial images. Distance from the centre is given from the middle of the box used to collect the pellets.

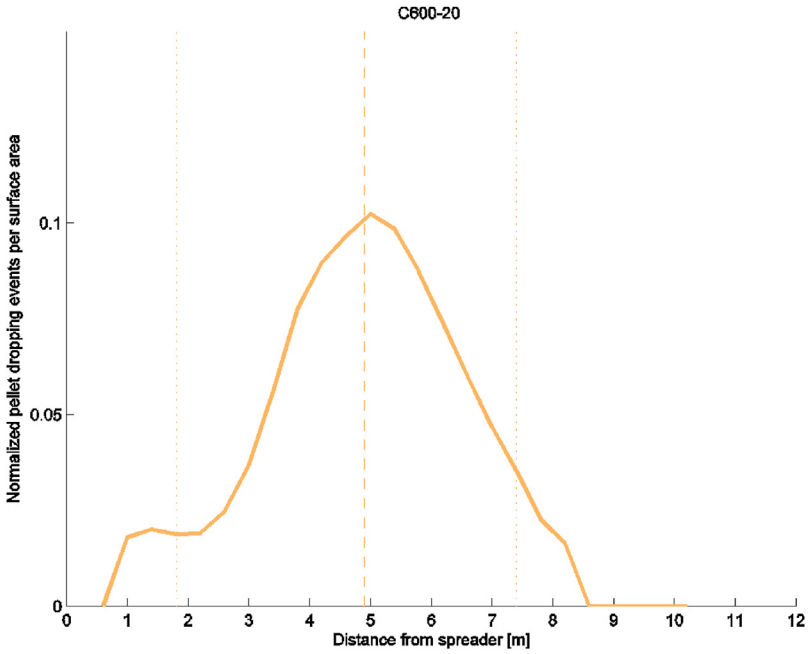

Fig. 12. Pellet splash detections from combined circumferential sectors as a measure of quantified pellet distribution from rotor spreaders. The area where 90% of the pellet splashes were detected was set between an inner limit, cutting off the 5% of splashes detected closest to the spreader, and an outer limit, cutting off the 5% of splashes detected furthest away from the spreader (dotted lines). The center of gravity of all the splash detections is indicated by the dashed line.

Table 2
Quantified pellet distribution from different spreader configurations. Distribution is defined between an inner limit, cutting off the 5% of splashes detected closest to the spreader, and an outer limit, cutting off the 5% of splashes detected furthest away from the spreader.

Spreader configuration	90% of pellets were detected within			Center of gravity [m]
	Inner limit [m]	Outer limit [m]	Difference [m]	
C600-16	2.6	6.2	3.6	4.3
C600-20	1.8	7.4	5.6	4.9
H450-16	1.4	5.8	4.4	3.5
H450-20	3.4	7.4	4.0	5.4
H600-16	1.8	6.2	4.4	4.0
H600-20	2.2	8.2	6.0	5.5

$$R = \frac{1}{\sum_{i=1}^{n} x_i} \sum_{i=1}^{n} x_i r_i \quad (1)$$

In Fig. 12 we show the radial pellet splash distribution for the C600 experiment (air speed 20 m s^{-1}). The inner limit radius, the outer limit radius and the center of gravity are displayed as dotted and dashed lines respectively. The results characterizing the pellet splash distribution for all the pellet spreader experiments are summarized in Table 2.

Winds and waves generally will have an impact on the actual pellet distribution, but the wind measured (Fig. 13) during our experiments were generally low (light air to light breeze) and we belief that the uncertainty and skewness in the observed distribution are larger influenced by the fact that the pellets often are spread in clustered batches with high pellet density. This corresponds with the results from simulation studies (Skøien et al., 2016b).

4. Conclusion/discussion

The aim we pursue with this paper is twofold. One is the investigation of the spreading performance and comparison of different spreaders. The other is the development and exploration of computer vision algorithms that allow to perform a more continuous or daily monitoring of the feeding process. Our applied method has some limitations concerning the amount of waves and wind it can cope with. As soon as for example the waves break on the surface the created splashes

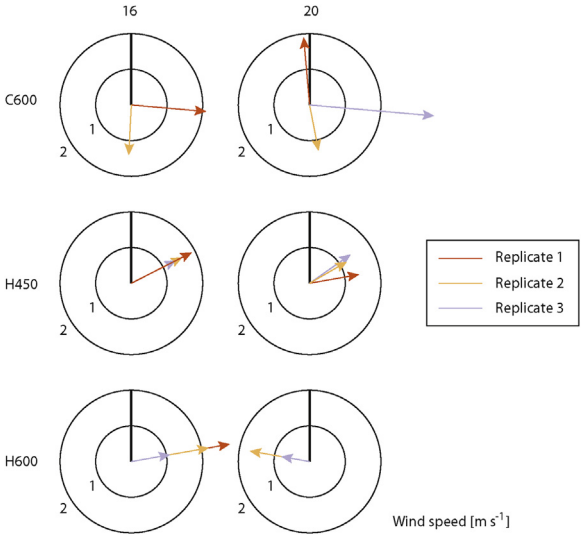

Fig. 13. Wind direction and speed during replicate 1 (dark orange), replicate 2 (light orange) and replicate 3 (light violet) of each experiment with rotor spreader models C600 (top), H450 (middle) and H600 (bottom) at blower air speeds 16 m s^{-1} (left) and 20 m s^{-1} (right). The feed pipe direction is indicated by the vertical black line in each diagram. Missing arrows mean the wind was too low to be measured at that time. (For interpretation of the references to color in this figure legend, the reader is referred to the web version of this article.)

would be falsely identified as pellet splashes. More advanced image based filtering and classification methods would be necessary to cope with such situations. Another possibility would be to track the visible flying pellets (using a high resolution camera in space and also in time) until they disappear. From the image processing analysis of the top-view video recordings of different feed pellet spreader configurations we found that images from an aerial camera platform, such as an UAV, can be utilized for characterizing feed pellet distribution of rotor spreaders. The method can be used in commercial salmon fish-cages without additional setup and therefore not disturbing the production. We observed that the used image resolution was high enough to be able to detect splashes that result from single pellets. However, exact pellet count is not possible due to the fact that pellet clusters easily result in a

larger uncountable non-homogeneous bigger splash where individual pellets cannot be distinguished. Some factors that make the image analysis of such aerial videos challenging come from the fact that the recorded scene is not static and the spreader center is moving within the video recordings and that different weather conditions can lead to quickly changing lighting conditions. The results in this study showed also a variation within replicated experiments. Therefore it is recommended that longer observation periods are used in future experiments using this method, increasing the data basis and thereby increasing the precision of the suggested method. The significance of this work comes from the fact that the performed measurement of the feed distribution – if done continuously and connected to a control system that targets the pellets to the fish – will help to reduce any environmental impact that results from uneaten feed and pollutes the water. We belief that the observation of the feeding process with an unmanned areal vehicle or a top-view camera mounted to a construction above the "hamster wheel" will be one way in the nearer future to continuously observe the pellet distribution on the surface of salmon fish cages and control the feeding by this information. A simple control mechanism for adjusting the feeding based on through-coming pellets and fish position is for example suggested in (Parra et al., 2018).

Authors contributions

Andreas Myskja Lien: Conceptualization, Methodology, Formal Analysis, Investigation, Writing – Original Draft, Writing – Review & Editing, Visualization, Project Administration, Funding Acquisition. Christian Schellewald: Software, Formal Analysis, Data Curation, Writing – Review & Editing. Annette Stahl: Software, Formal Analysis, Data Curation, Writing – Review & Editing. Kevin Frank: Conceptualization, Methodology, Validation, Formal Analysis, Writing – Review & Editing, Supervision, Funding Acquisition. Kristoffer Rist Skøien: Investigation, Writing – Original Draft. Jan Inge Tjølsen: Resources.

Acknowledgements

We would like to thank the crew at Korsneset fish farm for their assistance during the experiment and AKVA Group for providing the rotor spreaders. The research was funded by The Norwegian Research Council (project no. 235775/E40).

References

Alver, M.O., Alfredsen, J.A., Sigholt, T., 2004. Dynamic modelling of pellet distribution in atlantic salmon (Salmo salar L.) cages. Aquac. Eng. 31 (1–2), 51–72. https://doi.org/10.1016/j.aquaeng.2004.01.002. http://www.sciencedirect.com/science/article/pii/S0144860904000056.

Alver, M.O., Skøien, K.R., Føre, M., Aas, T.S., Oehme, M., Alfredsen, J.A., 2016. Modelling of surface and 3d pellet distribution in atlantic salmon (Salmo salar L.) cages. Aquac. Eng. 72–73, 20–29. https://doi.org/10.1016/j.aquaeng.2016.03.003. http://www.sciencedirect.com/science/article/pii/S0144860916300462.

Attia, J., Millot, S., Di-Poï, C., Bégout, M.-L., Noble, C., Sanchez-Vazquez, F.J., Terova, G., Saroglia, M., Damsgård, B., 2012. Demand feeding and welfare in farmed fish. Fish Physiol. Biochem. 38 (1), 107–118. https://doi.org/10.1007/s10695-011-9538-4.

Einen, O., Holmefjord, I., Åsgård, T., Talbot, C., 1995. Auditing nutrient discharges from fish farms: theoretical and practical considerations. Aquac. Res. 26 (9), 701–713. https://doi.org/10.1111/j.1365-2109.1995.tb00960.x.

Føre, M., Dempster, T., Alfredsen, J.A., Johansen, V., Johansson, D., 2009. Modelling of atlantic salmon (Salmo salar L.) behaviour in sea-cages: a lagrangian approach. Aquaculture 288 (3), 196–204. https://doi.org/10.1016/j.aquaculture.2008.11.031. http://www.sciencedirect.com/science/article/pii/S0044848608008533.

FAO, 2015. Food and Agriculture Organization of the United Nations. Available from: http://www.fao.org/fishery/statistics/global-aquaculture-production/en.

Geissmann, Q., 2013. OpenCFU, a new free and open-source software to count cell colonies and other circular objects. PLoS ONE 8, 1–10. https://doi.org/10.1371/journal.pone.0054072.

Juell, J.-E., 1995. The behaviour of atlantic salmon in relation to efficient cage-rearing. Rev. Fish Biol. Fish. 5 (3), 320–335. https://doi.org/10.1007/BF00043005.

Kadri, S., Huntingford, F., Metcalfe, N., Thorpe, J., 1996. Social interactions and the distribution of food among one-sea-winter atlantic salmon (Salmo salar L.) in a sea-cage. Aquaculture 139 (1–2), 1–10. https://doi.org/10.1016/0044-8486(95)01163-3.

López-Olmeda, J., Noble, C., Sánchez-Vázquez, F.J., 2012. Does feeding time affect fish welfare? Fish Physiol. Biochem. 38 (1), 143–152. https://doi.org/10.1007/s10695-011-9523-y.

Metcalfe, N.B., Thorpe, J.E., 1992. Early predictors of life-history events: the link between first feeding date, dominance and seaward migration in atlantic salmon, Salmo salar L. J. Fish Biol. 41, 93–99. https://doi.org/10.1111/j.1095-8649.1992.tb03871.x.

Noble, C., Kadri, S., Mitchell, D.F., Huntingford, F.A., 2008. Growth, production and fin damage in cage-held 0+ atlantic salmon pre-smolts (Salmo salar L.) fed either a) on-demand, or b) to a fixed satiation-restriction regime: data from a commercial farm. Aquaculture 275 (1–4), 163–168. https://doi.org/10.1016/j.aquaculture.2007.12.028. http://www.sciencedirect.com/science/article/pii/S0044848608000069.

Norwegian Directorate of Fisheries, 2013. Lønnsomhetsundersøkelse for matfiskproduksjon. https://www.fiskeridir.no/Akvakultur/Statistikk-akvakultur/Loennsomhetsundersoekelse-for-laks-og-regnbueoerret/Matfiskproduksjon-laks-og-regnbueoerret.

Oehme, M., Aas, T.S., Sørensen, M., Lygren, I., Åsgård, T., 2012. Feed pellet distribution in a sea cage using pneumatic feeding system with rotor spreader. Aquac. Eng. 51 (Suppl. C), 44–52. https://doi.org/10.1016/j.aquaeng.2012.07.001. http://www.sciencedirect.com/science/article/pii/S0144860912000568.

Olla, B., Davis, M., Ryer, C., 1992. Foraging and predator avoidance in hatchery-reared pacific salmon: achievement of behavioral potential. The Importance of Feeding Behaviour for the Efficient Culture of Salmonid Fishes. pp. 5–13.

Oppedal, F., Dempster, T., Stien, L.H., 2011. Environmental drivers of atlantic salmon behaviour in sea-cages: a review. Aquaculture 311 (1–4), 1–18. https://doi.org/10.1016/j.aquaculture.2010.11.020. http://www.sciencedirect.com/science/article/pii/S0044848610007933.

Parra, L., García, L., Sendra, S., Lloret, J., 2018. The use of sensors for monitoring the feeding process and adjusting the feed supply velocity in fish farms. J. Sens. https://doi.org/10.1155/2018/1060987.

Sandberg, Steinseide, 2017. Key Figures From Aquaculture Industry 2016. Report. (in Norwegian).

Sezgin, M., Sankur, B., 2004. Survey over image thresholding techniques and quantitative performance evaluation. J. Electron. Imaging 13 (1), 146–166. https://doi.org/10.1117/1.1631315.

Skøien, K.R., Alver, M.O., Alfredsen, J.A., 2015. Modelling spatial surface pellet distribution from rotary pneumatic feed spreaders. Proceedings of the 23rd Mediterranean Conference on Control and Automation (MED) 883–888. https://doi.org/10.1109/MED.2015.7158857.

Skøien, K.R., Alver, M.O., Zolich, A.P., Alfredsen, J.A., 2016a. Feed spreaders in sea cage aquaculture – motion characterization and measurement of spatial pellet distribution using an unmanned aerial vehicle. Comput. Electron. Agric. 129 (Suppl. C), 27–36. https://doi.org/10.1016/j.compag.2016.08.020. http://www.sciencedirect.com/science/article/pii/S016816991630299X.

Skøien, K.R., Alver, M.O., Lundregan, S., Frank, K., Alfredsen, J.A., 2016b. Effects of wind on surface feed distribution in sea cage aquaculture: a simulation study (accepted). European Control Conference (ECC) 1291–1296. https://doi.org/10.1109/ECC.2016.7810467.

Soille, P., 2003. Morphological Image Analysis; Principles and Applications. https://doi.org/10.1007/978-3-662-05088-0.

Szeliski, R., 2010. Computer Vision: Algorithms and Applications, 1st ed. Springer-Verlag, Berlin, Heidelberg. https://doi.org/10.1007/978-1-84882-935-0.

Talbot, C., Corneillie, S., Korsøen, Ø., 1999. Pattern of feed intake in four species of fish under commercial farming conditions: implications for feeding management. Aquac. Res. 30 (7), 509–518. https://doi.org/10.1046/j.1365-2109.1999.00369.x.

Talbot, C., 1993. Some biological and physical constraints to the design of feeding regimes for salmonids in intensive cultivation. Fish Farm. Technol. 19–26.

Thomassen, J., Lekang, O., 1993. Optimal distribution of feed in sea cages. Fish Farming Technology. Balkema Rotterdam, pp. 439–442.

Winther, U., Sandberg, M.G., Richardsen, R., Olafsen, T., Brandvik, R.K., Hauvik, J.-H., 2011. Potensial for økt verdiskaping i lakse-og ørretoppdrettsnæringen.

Ytrestøyl, T., Aas, T.S., Åsgård, T.E., 2014. Resource Utilisation of Norwegian Salmon Farming in 2012.